Label-Free Quantification of Soft Tissue Alignment by Polarized Raman Spectroscopy

Hui Zhou, Janny Piñeiro, Malisa Sarntinoranont, Ghatu Subhash and Chelsey S. Simmons[*]

Mechanical and Aerospace Engineering·, University of Florida, Gainesville, Florida, USA

Contact Email: css@ufl.edu

Keywords: polarized Raman spectroscopy, principal component analysis, extracellular matrix, protein alignment, anisotropic tissue

ABSTRACT

The organization of proteins is an important determinant of functionality in soft tissues. However, such organization is difficult to monitor over time in soft tissue with complex compositions. Here, we establish a method to determine the alignment of proteins in soft tissues of varying composition by polarized Raman spectroscopy (PRS). Unlike most conventional microscopy methods, PRS leverages non-destructive, label-free sample preparation. PRS data from highly aligned muscle layers were utilized to derive a weighting function for aligned proteins via principal component analysis (PCA). This trained weighting function was used as a master loading function to calculate a principal component score (PC1 Score) as a function of polarized angle for tendon, dermis, hypodermis, and fabricated collagen gels. Since the PC1 Score calculated at arbitrary angles was insufficient to determine level of alignment, we developed an Amplitude Alignment Metric by fitting a sine function to PC1 Score with respect to polarized angle. We found that our PRS-based Amplitude Alignment Metric can be used as an indicator of level of protein alignment in soft tissues in a non-destructive manner with label-free preparation and has similar discriminatory capacity among isotropic and anisotropic samples compared to microscopy-based image processing method. This PRS method does not require a priori knowledge of sample orientation nor composition and appears insensitive to changes in protein composition among different tissues. The Amplitude Alignment Metric introduced here could enable convenient and adaptable evaluation of protein alignment in soft tissues of varying protein and cell composition.

1. Introduction

Soft tissues like tendons, skin and cartilage support loads and facilitate tissue compliance for functioning of the human body. Tissue-engineered scaffolds composed of biomaterials and cells are often used for replacement of damaged soft tissues [1], and assessment of the structural organization of soft tissue constituents is essential for understanding their mechanical functionality and improving their design [2,3]. However, a critical issue in tissue engineering remains the development of engineered constructs with micro- and macroscopic alignment that mimics native tissue and maintains mechanical functionality [4,5]. Techniques to monitor alignment over time may help to develop more reliable and physiologically relevant tissue-engineered constructs. Further, monitoring the microstructural alignment of soft tissues at different stages of growth may provide information associated with aging and disease [6].

Many light-based and other imaging techniques have been used to characterize the alignment of structural proteins in soft tissues. These methods include histology [7], scanning electron microscopy [8], Förster resonance energy transfer [9] and magnetic resonance imaging [10]. However, these techniques are typically destructive, requiring dyes and equipment operation at non-physiological temperatures and pressures. To overcome these drawbacks, several label-free optical techniques have been adopted to measure protein alignment in tissues including second harmonic generation [6,11], polarized light microscopy [12], Fourier transform infrared (FT-IR) spectroscopy [13–15], and polarized Raman spectroscopy (PRS) [6,16]. PRS is of particular utility for analyzing molecular alignment as it relies on polarized laser to incite Raman scattering, and the orientation of vibrating molecules to the laser polarization direction can influence the Raman signal intensity [17]. Unlike other forms of spectroscopy, PRS can be performed in aqueous environment since the Raman scatter from water is weak, which enables

characterization of soft tissues in more native physiological conditions [18]. PRS has been exploited to characterize alignment of specific proteins in tissues such as collagen in bone [19], tendon [16,20,21] and articular cartilage [22][23] and elastin in ligaments [24]. Most prior studies have been focused on univariate analysis of the alignment of collagen molecules, e.g., relying on the single variable of the intensity or the area under the curve of the collagen amide I band, to quantify alignment.

While this single-variable approach attempted to characterize alignment in these collagen-rich tissues with sparse cell populations, it may not be applicable to other soft tissues with varying cell and protein composition [25]. The spectra from most soft tissues are composed of Raman bands from many macromolecules that make alignment analysis difficult. The spectra from soft tissues usually consist of both polarization-sensitive Raman protein bands that are correlated with the alignment and others that are irrelevant to structure-property of interest. The irrelevant bands may come from a mixture of various macromolecules (e.g., nucleic acid, fatty acid and carbohydrates) as well as the vibration modes of various proteins that are not sensitive to polarization. The intensities of those irrelevant Raman bands may vary both spatially and temporally, which can confound the intensity variations of polarization-sensitive Raman bands associated with alignment information. Hence, it is not useful to only use a single variable (e.g., intensity of amide I collagen band) to acquire the alignment in soft tissues with varying proteins. For example, the broad bands contributed by various constituents in Raman spectra confound the detectable collagen signal in complex tissues such as blood vessels [26] and kidneys [27,28].

To overcome the above limitations, multivariate analysis has been used to reduce the dimensionality of complex biological Raman data [29]. Principal component analysis (PCA), a common multivariate method, is often used to extract the most relevant information from Raman

spectra while ignoring irrelevant variation. By analyzing variances among the samples, PCA derives principal component (PC) loading spectra based on the contributions of the variance at each wavenumber, and spectral information is reduced to so-called PC Scores [30]. PCA can decipher the trends and patterns among different biological samples and separate them into distinct classes based on PC Scores, but additional steps are needed to correlate these classifications into quantifiable biochemical information. For example, PCA can separate the spectra of soft tissue with different polarization directions [22,31]; however, it cannot relate such separation to the alignment level of the tissue. There is a compelling need to develop new methods that can take advantage of multivariate statistical techniques and quantitate the alignment of proteins in soft tissues.

The aim of this work is to develop an analytical technique to leverage PRS data to quantitatively measure the alignment level of proteins in soft tissue. Here, the polarized Raman data of anisotropic soft tissue is used to train PCA to obtain a master loading function (Figure 1A). This trained master function is then applied to new data to determine the principal component score (hereafter "PC1 Score") for tissue samples relative to polarized incident and collected light. The resulting PC1 Score versus polarized angle is fitted using a sine function, and we hypothesize the alignment level of the tissue can be quantified by the amplitude of the sine fit, i.e., an Amplitude Alignment Metric (Figure 1). Schrof et al. [32] used a similar approach to characterize the level of anisotropy in compact bone by examining the amplitude of cosine fit, but similar univariate analysis of the intensity of the amide I Raman band only was inadequate to describe alignment in our complex skin samples.

To assess our hypothesis that the amplitude of the sinusoidal fit to PC1 Score correlates with the level of alignment in the sample, we use this PRS-derived Amplitude Alignment Metric

to assess alignment of a variety of soft tissues and tissue surrogates. We characterize simple, collagen-rich samples (i.e., rat tail tendon and fabricated collagen hydrogels) and complex layers of mouse skin with varying levels of cells and proteins. In each case, we will show that this Amplitude Alignment Metric is able to distinguish between anisotropic and isotropic samples via PRS without labels and without controlling protein composition, which suggests adaptability of this method to many soft tissues with varying cell and ECM composition. For validation, we compare our PRS-derived Amplitude Alignment Metric to an optical microscopy image-processing-derived Eccentricity Alignment Index. Statistical analysis comparing anisotropic and isotropic samples using these two metrics yields p-values that are the same order of magnitude, suggesting comparable discriminatory capability. Thus, we will show that the devised a PRS-based method to calculate an Amplitude Alignment Metric is an effective method for non-destructive quantification of alignment in soft tissues.

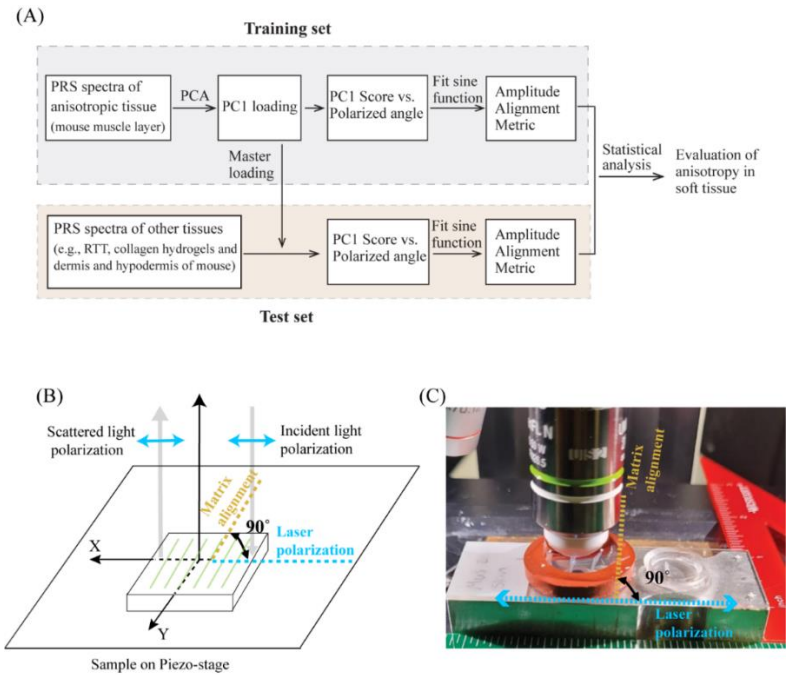

Figure 1. (A) Schematic of analytical steps for evaluation of tissue alignment via Polarized Raman Spectroscopy (PRS). *PCA = Principal Component Analysis, PC1 = Primary Principal Component, RTT = Rat Tail Tendon*. (B) Schematic of the experimental set-up of PRS. The polarized angle is adjusted by rotating the sample in XY plane with respect the laser polarization axis. (C) Image of experimental set up of mouse skin sample in a gasket

submerged in PBS with 90˚ Raman polarization configuration. Markings on rulers are 1/16".

2. Materials and methods

2.1. Sample preparation

Tissue samples. Animal work carried out in this study was approved by the Institutional Animal Care and Usage Committee at the University of Florida. Skin was collected from euthanized mice (CD1, male, 4-6 months old), fixed using 4% paraformaldehyde for 24 hours, and washed using phosphate-buffered saline (PBS) to remove excess fixative. Fixed skin samples were dehydrated by incubating in a series of graded ethanol (70%, 95% and 100%), xylene, and paraffin wax and then sectioned into approximately 10 μm-thick sections and collected on glass slides. The slides were dipped in xylene, a graded series of ethanol solution (100%, 90%, 70% and 50%), and PBS to remove the wax and rehydrate before PRS measurement.

Rat tail tendon (RTT) was extracted from the tails of Lewis rats (male, 4-8 months old) following methods previously reported [33]. Briefly, rat tails were disinfected with 70% ethanol and rinsed with deionized water. The skin and vertebrae of the tail were broken to expose fascicles that form the tendons. To remove any residual lipids, fascicles were rinsed with acetone followed by 70% isopropanol for 5 minutes each. Finally, fascicles of approximately 50 mm in length were placed on glass slides in quartz Petri dishes of PBS before PRS measurement.

Collagen gels. Collagen gels were fabricated following the methods previously described [34]. Briefly, to obtain a 4mg/mL collagen solution, rat tail collagen type-I stock solution (Corning) was diluted with 0.2% acetic acid (Glacial, Fisher Scientific) in PBS (InvitroGen, ThermoFisher). Then, the collagen solution was mixed at 4°C with a 5x DMEM-HEPES-Sodium Bicarbonate (7.5% (w/v)) solution (pH 7.4) in a 1:3 ratio to obtain a final 3 mg/ml collagen

precursor solution. Finally, collagen was allowed to polymerize at 37˚C for 35 minutes before adding PBS.

2.2. Polarized Raman measurements

Raman spectroscopy was performed in a Renishaw InVia spectrometer with a 532nm argon-ion laser at 50 mW power capacity. Crystal silicon with a fixed peak position (520.5 cm^{-1}) was used to calibrate the spectrometer for the Raman shifts before any measurements are taken on the test samples. Linearity of the Raman calibration is measured with the internal neon calibration source and, after correcting the off-axis and chromatic aberration, the calibration shows precision and accuracy of Raman wavenumbers better than 0.4 cm^{-1}. Prior to measurements on tissue samples, the Renishaw InVia was checked for instrumental polarization effects by measuring the depolarization ratios of CCl_4. Within experimental errors, these ratios were observed to be similar to those reported in literature, showing no significant polarization dependence of the Raman spectrometer. The Newton EMCCD platform was thermoelectrically cooled down to -100°C for negligible dark current. Raman spectra of the optical background were averaged out and subtracted from spectra of tissue samples. The Raman spectra on each tissue were recorded with a spatial resolution of approximately 1 μm through our 20× objective, numerical aperture (NA)=0.5, with a 200× total magnification. The spectra were acquired using a charge-coupled device (CCD) camera (Netwon EMCCD DU970P, Oxford Instruments plc, Tubney Woods, Abingdon, Oxon OX13 5QX, United Kingdom) with a grating of 1800 lines per mm, which yielded a spectral resolution of around 6.8 cm^{-1}. The spectra were collected using WIRE® 4.4 workstation software (Renishaw plc, England) in extensive mode ranging from 590 cm^{-1} to 2200 cm^{-1}. Measurements were performed at room temperature with samples submerged

in PBS, and a 10 μm region of interest (ROI) was scanned at a step size of 1 μm, i.e. 11 acquired spectra, with 2 ROIs for each sample. 12 accumulations each with an acquisition time of 10s were used for each location. Thermal effects such as heating were neglected under the assumption that the PBS-immersed sample dissipated heat rapidly, as expected for water. The incident laser was initially polarized horizontally (X-direction, see Figure 1B). A linear polarizer was placed behind the Rayleigh filter in the scattered beam to select the parallel scattered light component with respect to the polarization of incident light. Thus, the PRS measurements were conducted with both the incident laser and detected laser always polarized along X-direction (see Figure 1B). By rotating the sample, we varied the polarization angle between laser polarization direction and the sample alignment axis. The polarization angle was varied from 0˚ to 180˚ in 30˚ increments.

2.3. Data processing

The raw spectra were subtracted from background fluorescence in WIRE® 4.4 software (Renishaw plc, England) using an eleven-order polynomial fit. The resulting spectra were then truncated from 1400-1800 cm^{-1} and subtracted from background spectra obtained from blank glass slide submerged in PBS. These spectra were further smoothed by Savitzky-Golay filters with polynomial order of 3 and window size of 11 in Matlab® (R2020a, The MathWorks, Inc., Natick, Massachusetts, United States). Then the smoothed spectra were processed with Standard Normal Variate (SNV) normalization in Matlab®. Descriptive and multivariate statistical PCA analysis (Origin2020, OriginLab) of the muscle layer spectra provided a principal component (PC1) that transformed spectra of different polarized angles into a single score variable that covered the maximum variation (~85%) of the spectra data. The loading curve of this PC1 was

treated as a master loading function that was fed into PCA analysis to transform the spectra of all other tissue samples. The output of the loading function (i.e., PC1 Score) as a function of polarized angle for each location was fitted with a sine function:

$$y = y_0 + A \sin\left(\frac{\pi(x - x_c)}{90°}\right) \quad (1)$$

where y is the PC1 Score, y_0 is y-offset for the sine fit, A is amplitude of the sine fit, x is the experimental polarization angle (in degrees) between the sample alignment axis and laser, and x_c is the phase shift. Since the orientation of an arbitrary sample is not known a priori, the phase shift, x_c, is fixed prior to sine fitting by calculating where the maximal difference of PC1 Score occurs between experimental polarization angles separated by 90º for a given tissue sample. For example, if the largest difference between PC1 Score is observed between 30˚ (positive PC1 Score) and 120˚ (negative PC1 Score), then x_c = -15˚. The procedure to fix the phase shift is consistently applied to both anisotropic and isotropic samples to compare the sine fit amplitude across different tissue samples. The amplitude of sine fit, A, becomes the Amplitude Alignment Metric used for quantifying the alignment level in soft tissue samples via PRS.

2.4. Phase contrast imaging

A Keyence inverted microscope (Model BZ-X810; Itasca, Illinois, U.S.A.) was used for this study. The microscope set-up and the phase ring of the objective (Nikon, objective type Plan Fluorite, numerical aperture (NA) of 0.60, and a 3.3-2.2 mm working distance) provided phase contrast imaging on a dark background, such that the increases in diffraction when passing through the biologic tissue appear as increases in detected light by the CCD. Tissue that had higher scatter intensity appeared brighter. A high power, ×40 magnification, was used to acquire

phase contrast images with a resolution of 1920 × 1440 pixels (physical size = 500 μm × 374 μm) on each tissue sample and the grayscale phase contrast images were used for image analysis and alignment determination later.

2.5. Image analysis and statistical analysis of alignment metrics

Regions of interest in each tissue sample (78 pixels × 78 pixels) were cropped and processed with a binary mask in Fiji (NIH, Bethesda, MD, USA) (Figure 2A-B). Binary images were then fed into the *Directionality* plugin (Jean-Yves Tinevez), a Fast Fourier Transform-based method to determine frequency of features occurring within 30˚ increments. A polar histogram of fiber orientation was constructed using these 30º bins, and an ellipse was fitted to the distribution using a direct least squares method [35] in Matlab® (Figure 2C-D). The eccentricity of the fitted ellipse was calculated according to the standard definition: *Eccentricity* $= \sqrt{1 - \left(\frac{b}{a}\right)^2}$ where *a* and *b* represent the length of long axis and short axis of the fitted ellipse, respectively. Here, we refer to the calculated eccentricity as the Eccentricity Alignment Index which ranges between 0 to 1, where 0 describes a perfect circle and thus perfectly isotropic samples and 1 describes a straight line and thus perfectly aligned samples.

Tukey-Kramer's post-hoc test and Student t-test were used to determine statistically significant differences among the skin layer samples and between the collagen samples, respectively, in JMP statistical software (version 4.0.4; SAS Institute, Inc.).

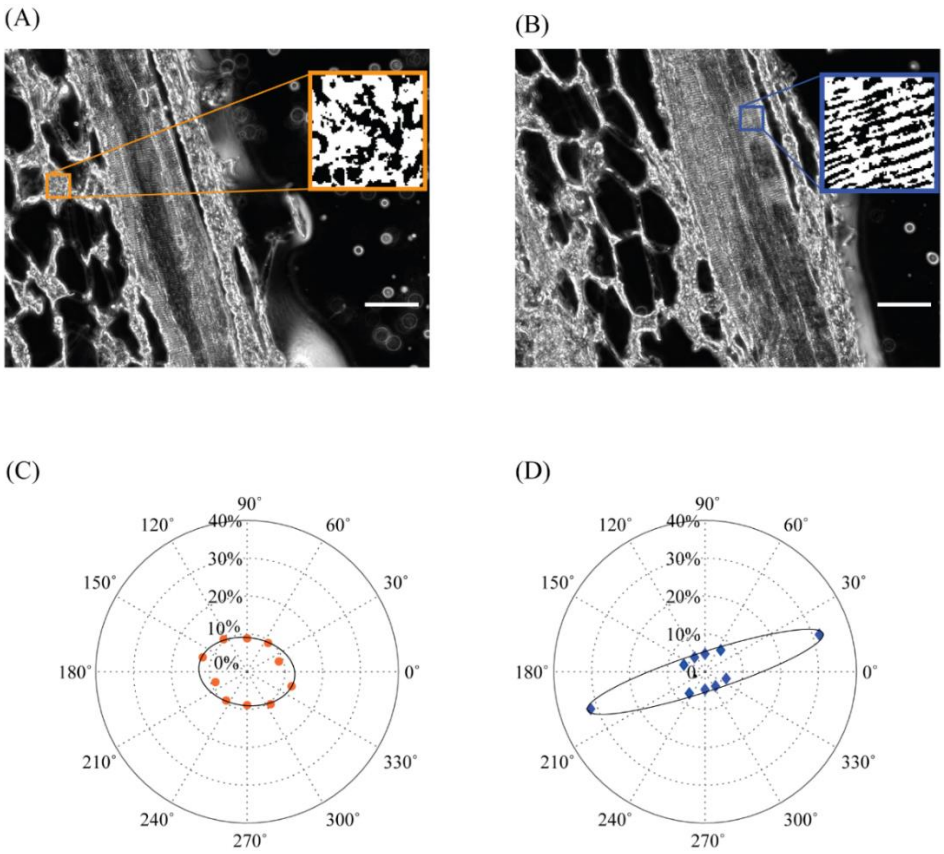

Figure 2. Phase images of mouse skin for directionality analysis on (A) isotropic layer and (B) anisotropic layer, respectively (scale bar = 20 μm). The insets are binary images of cropped regions (each: 12.5 μm × 12.5 μm) for analysis. Phase images were characterized by plugin Directionality in Fiji. Examples of polar orientation histogram of (C) isotropic tissue (hypodermis) and (D) anisotropic tissue (muscle) for acquiring the Eccentricity Alignment Index. Angle labels of the polar histogram indicate the absolute angle between the calculated orientation of image features and horizonal axis, and the radial labels indicate the percentage of features in the given direction.

3. Results

3.1. PCA reveals anisotropy of muscle layer in mouse skin

To train a loading function that could distinguish the orientation of intact soft tissue structure, polarized Raman spectra were collected from mouse skin in a region with a known alignment, the muscular *parniculous carnosus* layer (Figure 3A, gross alignment is perpendicular to the striations of muscle layer in bright field imaging). A rotation of the sample alignment axis with respect to the polarization axis of the laser (recall the incident and collected axes are the

same) in steps of 30˚ was performed on ROIs. As we changed the polarized angle, Raman intensity of a Raman band changes and "shifts" proportionally, but this is different from a traditional Raman shift. The frequency of a Raman band will not shift unless there is a thermal change or residual stress in tissue and such changes do not occur in our study. The major changes in intensities of amide-I-related bands are highlighted in the Figure 3B inset, which are also the regions that have highest weight (~0.1-0.2) in the loading curve and are highlighted in Figure 3C. Generally, intensities of Raman bands in aligned regions were maximal at 0º (or 180º) and minimal at 90º, similar to other reports [31,36]. To test if PCA could be used to distinguish the spectral differences at different polarized angles, the Raman intensities of Raman bands between 1400- 1800 cm^{-1} were analyzed. Most of the variability (86%) in the data are explained by the first principal component (PC1), so the loading function associated with PC1 (Figure 3C) was declared the "master loading function" and used in subsequent analysis. When applying the PC1 loading function to PRS spectra acquired at different angles between the sample and laser polarization, the PC1 Score exhibited significant differences (Figure 3D).

The PC1 loading curve (Figure 3C) reveals the Raman bands that exhibit the greatest contribution to the PC1 Score are 1445 cm^{-1} ($\delta(CH_2)$), 1465 cm^{-1} (lipids), 1605 cm^{-1} (phenylalanine), 1630-1656 cm^{-1} (amide I ν(C=O) collagen), and 1665-1685 cm^{-1} (amide I ν(C=O) collagen). This indicates that those bond vibrations may have a preferential orientation and that the intensities associated with these vibrational modes are orientation dependent, which we hypothesize can be used as a measure of alignment across biological tissues as most proteins include these bonds.

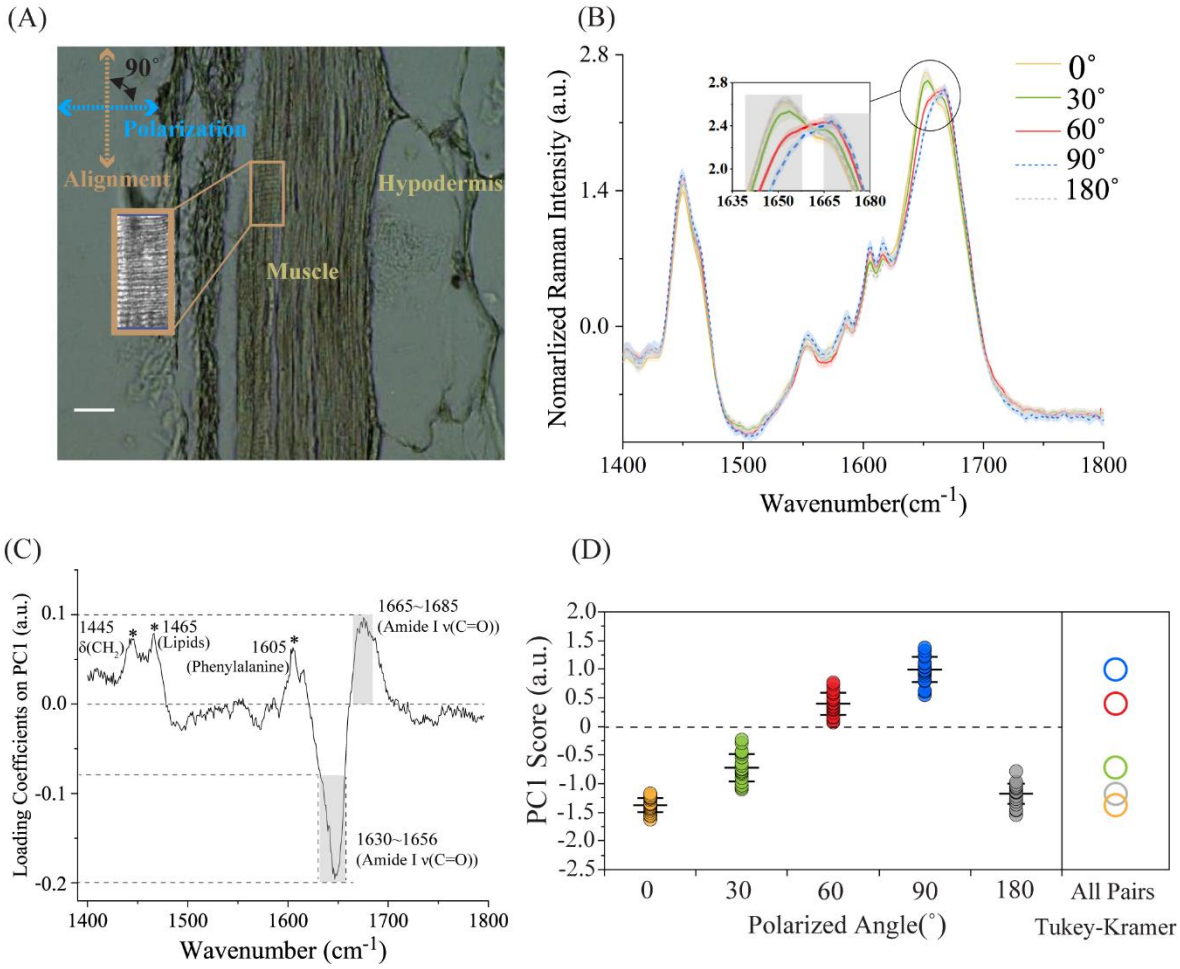

Figure 3. Principal Component Analysis (PCA) reveals anisotropy of muscle tissue. (A) Bright field image of muscle layer for PRS measurement in a 90˚ polarized configuration (scale bar: 10 μm). Inset: ~ 2x zoom of phase contrast image of striations in the muscle layer. (B) The mean and the standard deviations of Raman spectra (n = 22 technical replicates) of different laser polarization angles with respect to the mouse muscle layer axis in the 1400-1800 cm^{-1} range were used for PCA. Solid lines represent SNV normalized mean spectra and shaded areas represent corresponding standard deviation. Inset: the major differences are shown in amide I 1630-1656 cm^{-1} and 1665-1685 cm^{-1}. (C) Principal component loading curve for primary principal component (PC1) was determined via PCA of 22 replicates at 5 angles (110 spectra total). The resulting loading curve accounts for 50% of the variance among angles. Peaks in the loading curve (e.g., 1445, 1465, 1605, 1630-1656 cm^{-1} and 1665-1685 cm^{-1}) correspond to CH_2, lipids, phenylalanine and Amide I bands, respectively, which are known to be present in soft tissue. (D) PC1 Score calculated using the PC1 loading curve for Raman spectra of a sample, acquired at different polarized angles. Intersecting circles represent similar sample means while all non-intersecting circles represent significantly different sample means via Tukey-Kramer comparison for all pairs ($p < 0.0001$, n=22 for each angle). Error bars indicate one standard deviation of the mean.

3.2 Anisotropy and isotropy in other tissues captured by the trained model

With the PC1 Score established to distinguish sample orientation, we designated the PC1 loading function as the "master loading function"; that is, we then used the PC1 Score trained on aligned intact tissue to test spectral variation and potential anisotropy of other unrelated samples. The PC1 Score of RTT via the master loading function showed significant difference among different polarized angles (Figure 4A), reflecting the known anisotropic structure of mostly collagen proteins in RTT [16]. In contrast, the PC1 Score of isotropic collagen gels using the master loading function showed no significant differences among the polarized angles (Figure 4B-4D). The differing structure of RTT and collagen hydrogel was confirmed by a common image processing technique: FFT-based image processing to determine alignment of microscale features. Though RTT and synthetic collagen gels are largely acellular, the master loading function trained using aligned muscle layer data is still able to capture (an)isotropy in these samples of relatively simple composition.

Though showing some differences of PC1 Score between two polarized angles, dermal and hypodermal layers of mouse skin did not show consistently significant differences among all polarized angles (Figure 4C-4D), in contrast to the observation in the muscle layer of the same tissue (Figure 3D). The lack of consistency for spectral variations among all polarized angles implies that protein structure in those two layers was isotropic, and this was verified by image processing of unstained sections from the same tissue. Though the master loading function was trained by spectra acquired on the muscle layer, the weighted bands include CH_2, lipids, phenylalanine, amide I bands, common to most soft tissue and protein-derived scaffolds, and thus retain relevance for other regions and tissues.

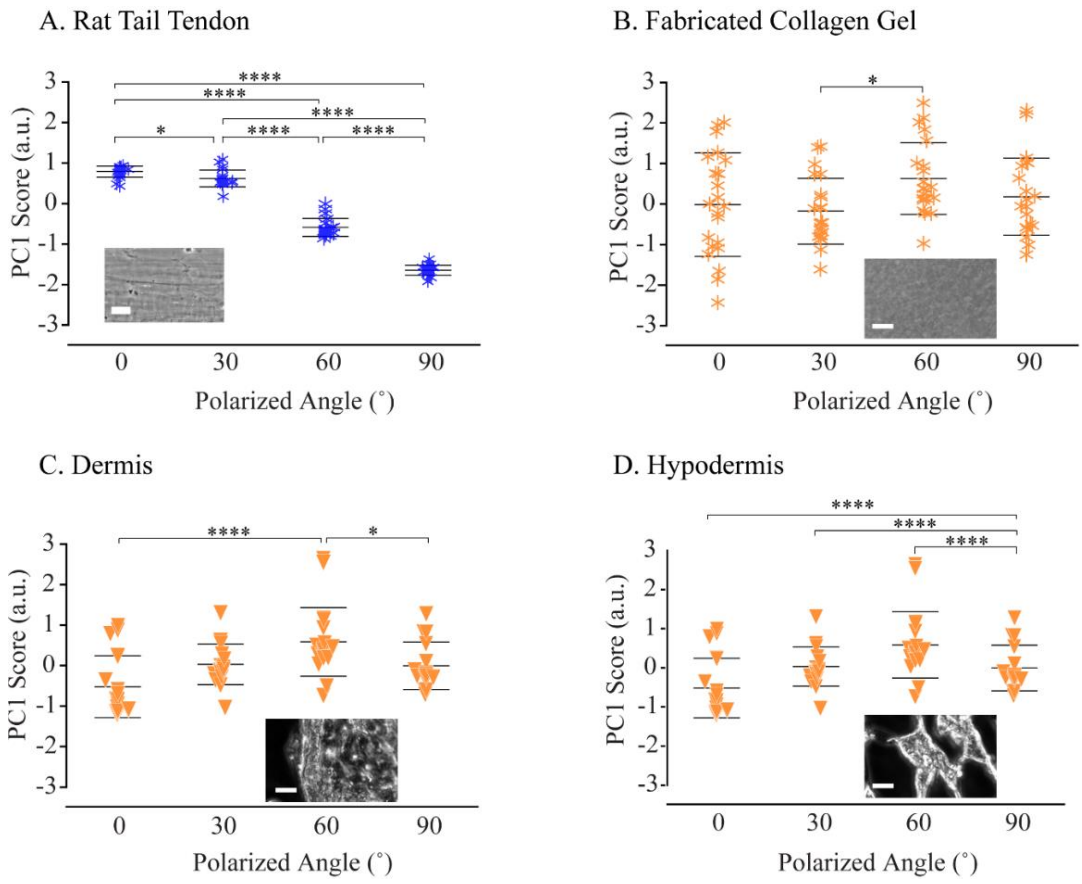

Figure 4. Anisotropy and isotropy in other tissues are captured by the trained master loading function and resulting PC1 Score of (A) RTT, (B) fabricated collagen hydrogel, (C) dermis and (D) hypodermis of mouse skin. The insets in (A)-(D) are phase images of the corresponding samples (scale bars: 10 μm). Anisotropic tissue (RTT) yields significant differences in PC1 Score among all polarization angles, while isotropic tissue samples (collagen hydrogel, dermis and hypodermis) typically do not have significant differences among all the polarization angles. ****=p<.0001, *=p<.05, as determined by one-way ANOVA followed by Tukey-Kramer's post-hoc test (**n**=**22** technical replicates for each angle). Error bars indicate one standard deviation of the mean. Blue = anisotropic tissues; orange = isotropic tissues; ✱ = collagen samples; ▼ = mouse skin samples

3.3. Amplitude Alignment Metric derived from the amplitude of PC1 Score sine fit

Since comparison of the PC1 Score between two arbitrary angles appeared insufficient to establish (an)isotropy, we sought to establish an analytical method that could evaluate PC1 Score as a function of multiple angles between sample and laser polarization. This is especially critical to the intended future use case where the biological sample orientation may not be predictable *a priori*. Thus, we fit sine curves to the PC1 Score as a function of polarized angle for each ROI

using Equation 1. The resulting sine fits reasonably captured the variations in Raman intensities of aligned proteins in tissue (Figure 5).

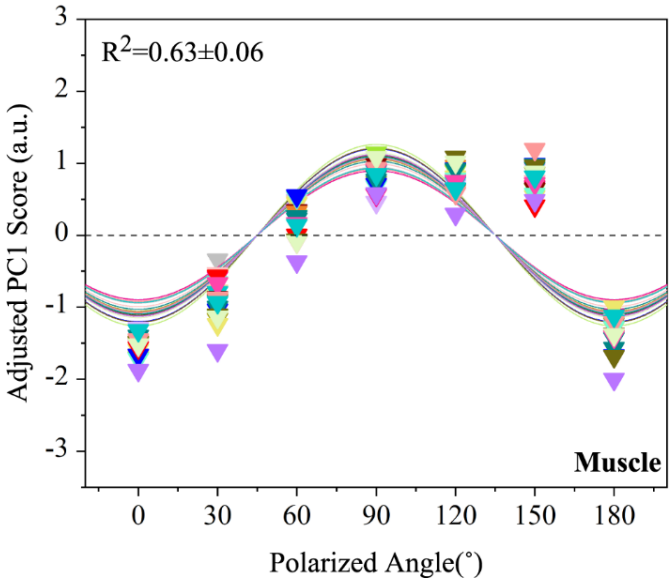

Figure 5. Sine fit captures the oscillation pattern of PC1 Score with the polarized angle in anisotropic muscle. After polarized Raman spectroscopy, the PC1 Score was fitted by sine function $y = y_0 + A \sin\left(\frac{\pi(x-45^\circ)}{90^\circ}\right)$. See details in text on Equation 1. Phase shift was set to 45º, as indicated, and the resulting sine fits and data are shifted by y_0 for clarity (i.e., Adjusted PC1 Score). R-square is shown by mean ± standard deviation (SD). The curves show a maximum PC1 score when the polarization of the laser is perpendicular to the muscle layer axis. Matching colors indicate the same measurement location at different angles used to fit each sine curve.

We repeated this process of fitting the sine curves to PC1 Score as a function of laser polarization angle for all other samples (Figure 6). Isotropic samples show poor sine fits with smaller amplitude (Figure 6B-D) while the anisotropic sample shows good sine fits with higher amplitude (Figure 6A). For different structures of the same composition, we found a significantly higher mean of the Amplitude Alignment Metric in aligned rat tail tendon compared to isotropic collagen gel (Figure 7A). For tissue regions with different structure and different composition, we were still able to distinguish a significantly higher Amplitude Alignment Metric in the aligned muscle layer compared to both the isotropic dermal and the isotropic hypodermal layers (Figure 7B). Hence, the amplitude of sinusoidal fit for PC1 Score reflects the degree of alignment of proteins in tissue and select fabricated protein-derived scaffolds.

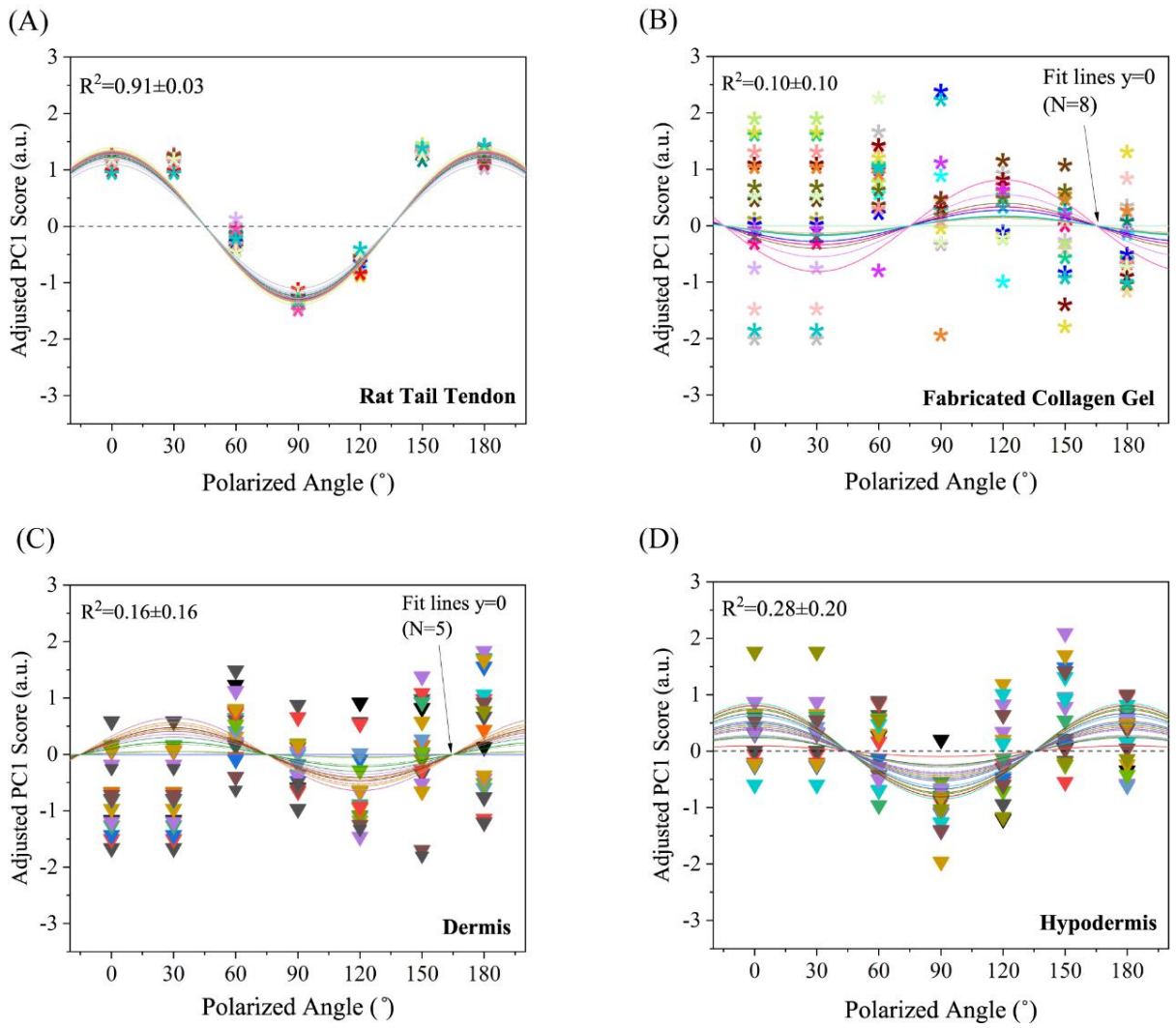

Figure 6. PC1 Score for anisotropic tissue (A) yields a reasonable sine fit whereas PC1 Score for isotropic tissue samples (B-D) yields a poor sine fit. R-square is shown by mean±SD in each figure. PC1 Score is fitted by the sine function $y = y_0 + A \sin\left(\frac{\pi(x-x_c)}{90°}\right)$ where y = PC1 Score and x = Polarized Angle. Additional details for Equation 1 are in the text. Data and sine fits are shifted by y_0 for clarity (i.e., Adjusted PC1 Score). Matching colors indicate the same measurement location at different angles used to fit each sine curve. ∗= collagen samples; ▼ = mouse skin samples

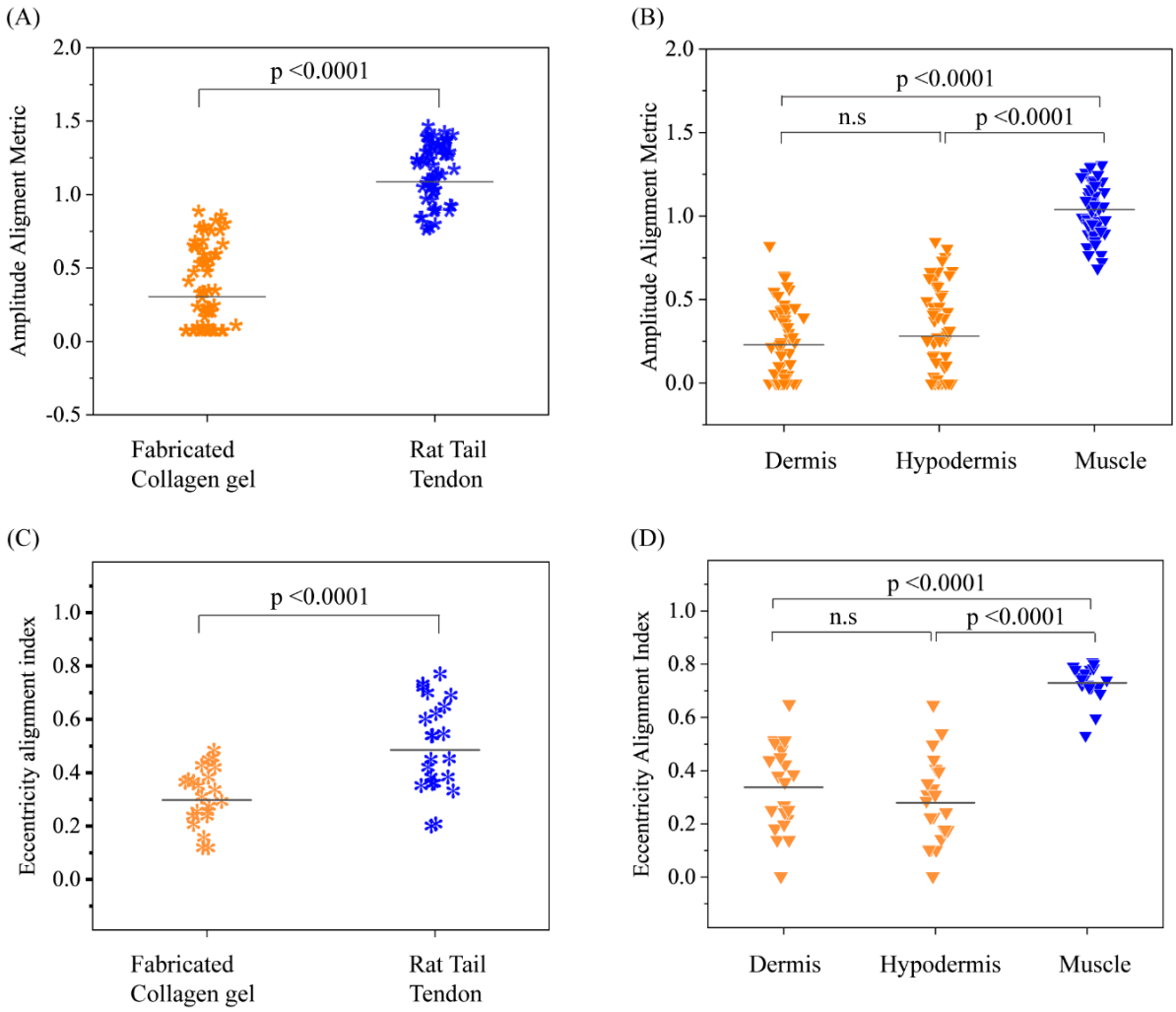

Figure 7. PRS analysis (Amplitude Alignment Metric) and phase imaging analysis (Eccentricity Alignment Index) yield similar comparisons between anisotropic tissue and isotropic tissues. (A) The Amplitude Alignment Metric calculated by our analysis of PRS data is significantly higher for anisotropic collagen than isotropic collagen via Student t-test (n=66 technical replicates). (B) The Amplitude Alignment Metric is significantly higher for aligned proteins in the muscle layer compared to unaligned proteins in dermal and hypodermal layers of mouse skin via Tukey-Kramer's multiple comparisons test (n=66 technical replicates, n.s. = not significant). (C) The Eccentricity Alignment Index calculated by image processing of phase contrast images is significantly higher for anisotropic collagen compared to isotropic collagen via Student t-test (n=22 technical replicates). (D) The Eccentricity Alignment Index is significantly higher for aligned proteins in the muscle layer compared to unaligned proteins in dermal and hypodermal layers of mouse skin via Tukey-Kramer's multiple comparisons test (n=22 technical replicates, n.s. = not significant). Blue = anisotropic tissues; orange = isotropic tissues; ∗= collagen samples; ▼ = mouse skin samples

4. Discussion

We have successfully devised an experimental and analytical procedure to quantitatively assess the level of alignment in tissue and protein-derived scaffolds without physical contact or any label. By utilizing PCA of PRS spectra, we were able to identify peaks in the spectra that corresponded to alignment of biological proteins. Previous studies on quantifying the orientation of proteins (e.g., collagen) in tissues were based on univariate analysis of a pre-identified variable, such as the peak intensity of the amide I band [16] or peak intensity ratio of amide III doublets [19]. However, deconvolution of Raman bands often exacerbates uncertainty in data, especially when biological soft tissues are not collagen-rich. Since PCA is unsupervised, we did not have to specify peaks of interest a priori and the loading function is more forgiving with noisy biological data than deconvolution that attempts to identify a single intensity peak. In addition, differences in protein content are likely to affect a single PRS peak more than orientation.

To surmount these issues of variance and protein content, we were able to use PCA to identify a master loading function, based on the PC1 loading curve, that preferentially weighted broad peaks related to orientation-dependent vibrational modes rather than relying on deconvolution of pre-selected peaks. Without prior knowledge, PCA identified two amide I bands, one of lower energy at 1630-1656 cm^{-1} (amide I ν(C=O)) and the other of higher energy at 1665-1685 cm^{-1} (amide I ν(C=O)), that have strong orientation dependencies relative to the laser polarization (Figure 3C). Both parallel and perpendicular carbonyl groups along protein backbone chains contribute to our ability to distinguish the overall macroscopic alignment of proteins. For example, in muscle tissue, the maximal intensity of lower energy amide I band occurs at 0˚ due to carbonyl groups oriented parallel to protein backbone while the maximal

intensity of higher energy amide I band occurs at 90˚ orientation due to perpendicular-oriented carbonyl groups (Figure 3B). Moreover, the angle at which the maximal intensity of lower energy amide I band occurs in myosin-rich muscle is different from that in collagen-rich RTT, which has been seen in other studies [21] due to different orientations of carbonyl groups in different proteins [6,16,21,36,37]. These different trends result in out-of-phase PC1 Score distributions for muscle and RTT. For the muscle layer, the PC1 Score is maximal at 90˚ when muscle fibers are perpendicular to the laser polarization (Figure 3D), while PC1 Score is maximal at 0˚ for collagen fibers of RTT, i.e., parallel to the laser polarization (Figure 4A). Despite these different distributions, using the amplitude of the sine fit to PC1 Score as a metric still quantifies the overall alignment of proteins in different soft tissues.

Moreover, our master loading function also includes weighting for the $\delta(CH_2)$ band. Janko et al. [20] showed a small variation of intensity of $\delta(CH_2)$ band as they rotated bovine Achilles tendon. In a univariate analysis, Van et al. [6] directly treated the $\delta(CH_2)$ band as insensitive to polarization based on the results of Janko and eliminated otherwise observable variation. Our spectra showed that the $\delta(CH_2)$ band displayed a similarly weak anisotropic Raman response in muscle and RTT; however, the value of determining a loading function via PCA is that it can emphasize any band that displays an anisotropic response, even if this response is slight. Our data suggests that some of the methylene groups of the amino acid side-chains, e.g., from proline, may be oriented, as reported previously in other studies [36] and thus contributing to the loading function.

The amide I, lipids, phenylalanine and CH_2 bands identified by unsupervised PCA are present in most biomacromolecules (e.g., proteins) of soft tissues [22,36,38,39]. Importantly, the master loading function appears to characterize the alignment level in tissue samples of widely

varying protein composition. This suggests that the master loading function and resulting PC1 Score reflects the protein alignment more than protein composition. RTT and fabricated collagen hydrogels have much more collagen than the dermal muscle layer, 86% versus 72%, respectively [40,41]. RTT and hydrogel samples are acellular while the dermal and hypodermal layers contain different cell types. In mouse skin, muscle layer contains more contractile protein fibers than dermis and hypodermis. Our findings suggest that changes in cell number and intra/extracellular protein composition in those soft tissue samples are unlikely to limit the utility of the PC1 Score. It would be interesting to see if such method can be applied to characterize the alignment in engineered tissue constructs, in which cell number and intra/extracellular protein composition vary during the process of tissue maturing.

For anisotropic samples such as muscle and RTT, PC1 Score does not linearly increase with the polarized angle (Figure 3D and Figure 4A). Furthermore, significant differences between angles in isotropic samples observe no useful identifiable pattern (Figure 4B-4D). Taken together, we concluded that comparison of one or two measurements at arbitrary polarization angles would not be sufficient to quantify sample alignment. Since Raman laser response of tissues in relation to polarized angles have been observed to be sinusoidal or cosinusoidal [16,21,32], we used a sine function to fit the PC1 Score in relation to polarized angles. The value of R^2 for the sinusoidal fits indicated a reasonable fit for PC1 Score of the anisotropic muscle layer (Figure 5, $R^2 = 0.63 \pm 0.06$ and anisotropic RTT (Figure 6A, $R^2 = 0.91 \pm 0.03$). Unsurprisingly, sinusoidal fits were poor for isotropic samples because captured "oscillations" as a function of polarization angle were just variability of the complex biological samples. Since proteins are randomly oriented with respect to millimeter-scale organization of tissue for isotropic samples, the phase shift is unlikely to have any physical meaning and was set

according to procedures in the Method section. Since R^2 correlated with the amplitude of sine fit (Supplemental Figure S1), a better sine fit and a higher amplitude. To correlate the sinusoidal Raman response to alignment, here we used the amplitude of the sinusoidal fit as an Amplitude Alignment Metric to quantify the alignment level in soft tissues.

When we compared the amplitude of sine fit within the collagen groups (RTT and fabricated collagen hydrogels) and among different layers of mouse skin, we found that the Amplitude Alignment Metric was sufficient to distinguish sample alignment. For the collagen samples with different structures, anisotropic RTT showed significantly higher amplitude compared to that of isotropic fabricated collagen hydrogels (1.09 ± 0.20 vs. 0.31 ± 0.27, $p < 0.0001$) in Figure 7A. Smaller amplitudes of sine fits indicated the insensitivity of PC1 Score to different polarized angles, confirming random orientation of fibers in fabricated hydrogels. Indeed, fabricated collagen hydrogels were formed from RTT isolates, largely preserving collagen protein composition while disrupting higher-order structure [33,42]. For different layers of muscle skin that consists of different compositions and structures, the anisotropic layer also displayed significantly higher amplitude than isotropic layers (Figure 7B, $p < 0.0001$). Importantly, with our method, we could distinguish anisotropic from isotropic tissue samples whether the samples consist of the same protein composition (plain collagen group) or not (different layers of muscle). This reinforces the utility of the master loading function emphasizing amide I and CH_2 bands that are sensitive to polarization and orientation and that are common in both cells and matrix of soft tissues.

To validate our method against other metrics of alignment used by the tissue engineering community, we compared our Amplitude Alignment Metric to an anisotropy index derived from image processing of micrographs (Figure 7C-D, Figure 2). Histological and

immunohistochemical labeling of tissue has been instrumental in assessing the alignment of proteins in tissue constructs [43,44], often combined with Fast Fourier Transform (FFT) algorithms to quantify fiber orientation [45–50]. For example, Chen et al. [49] applied 2D FFT-based algorithm on microscopy images of tissue engineered cartilage hydrogels to obtain the histogram of collagen fiber orientation. When we compared our non-destructive, PRS-based Amplitude Alignment Metric to an image processing Eccentricity Alignment Index, the p-values indicating statistical significance were of similar value, suggesting the indices possess similar discriminatory capacity. Here, we aimed to provide a characterization of the tissue sample orientation in label-free fashion without a priori knowledge of sample orientation nor composition. This can eliminate the need for tissue staining in histological and immunohistochemical methods. Those methods typically require labels beyond fixation processes [51,52]. For example, haematoxylin and eosin (H&E) staining can dye all the cellular components and connective tissues irrespective of molecular composition. However, PRS requires no labeling and has a high molecular specificity. As to immunohistochemical methods, they usually require a specific biomarker panel that must be first carefully selected. Often, the antibody-based biomarkers are expensive, and inappropriate selection of them can compromise analysis.

Though multiple analytical steps are required to derive the Amplitude Alignment Metric, our PRS-based method affords a number of advantages over other methods attempting to characterize tissue alignment. In comparison with other available methods of quantifying protein alignment in soft tissues, such as polarized fluorescence microscopy, PRS requires neither labeling during preparation nor sample contact and is non-destructive. Moreover, the effects of PBS buffer solution and culture medium on Raman analysis are both minimal, which makes

polarized Raman highly suitable for aqueous studies in tissues. In addition to the expected strong Raman peaks due to water at around 1640 cm^{-1}, the cell culture medium (DMEM/F-12) contributes additional weak peaks at around 1046, 1305 and 1454 cm^{-1} for both visible laser (488nm) and infrared laser (785nm) [53,54]. Similar to PBS buffer solution, the cell culture media can be subtracted without compromising any spectral features of proteins in tissues in the range 1400-1800 cm^{-1} and thus is unlikely to affect the dispersion of PC1 Score per angle and anisotropy resolution in this amplitude method. Due to such minimal interference, the polarized Raman spectroscopy has the potential to characterize tissues in the conventional tissue region (600-1800 cm^{-1}) and higher wavenumber region (2,700–3,500 cm^{-1}). Contrary to polarized Raman, conventional polarized infrared (IR) spectroscopy would encounter strong IR signal of liquid water, which makes interpretation of tissue and cell signals difficult in some regions. While advanced IR spectroscopy can examine tissue samples in aqueous solution with super-resolution (20 nm-500 nm) in recently developed techniques [14,15], conventional polarized IR still derives spectral data of tissue 'complementary to' but not 'instead of' polarized micro-Raman spectroscopy. More importantly, our master loading function that captures the most significant anisotropy works for complex soft tissue such as skin that consists of layers of different degrees of alignment as well as different compositions (cell and proteins).

While previous studies have focused specifically on the collagen orientation in collagen-rich tissues [16,22], we have worked to quantify the anisotropy of proteins in a variety of soft tissues, including fat, muscle and fibrous tissue, by leveraging multivariate PCA. For complex tissues, it is unreliable to quantify the alignment via a single Raman peak since the wavenumber of that Raman peak may vary across different proteins containing in soft tissue. The loading function derived from PCA identifies and respectively weights *all* anisotropic Raman bands that

are useful for quantifying the alignment of soft tissue. While the loading function was derived from muscle tissue, the different bond vibration modes emphasized by the master loading function are common among biological tissues and appear applicable to other soft tissues of varying composition. Although the orientations of these vibrating bonds relative to protein backbone chains may be different in different tissues, each oriented bond contributes to the degree of anisotropy in tissue. Our method transforms their intensities into a single metric to quantify the degree of overall protein alignment in soft tissue.

Moreover, varying cell and intra/extracellular protein composition in different soft tissue samples are unlikely to limit the utility of our method. Hence, this PRS technique coupled to PCA offers the opportunity to quantify the anisotropy in living tissues (e.g., engineered musculoskeletal tissue [55]) that consist of multiple ECM components that may be changing over time. This analysis could also be applied to complex scaffolds such as cell-derived matrices, which are more physiologically relevant than purified matrix proteins that lack the complex tissue composition seen *in vivo*. By accommodating changing cell and ECM constituents, this technique could likely evaluate the degree of alignment in engineered tissue constructs longitudinally with time. Furthermore, the evaluation of structures occurs at the molecular level with our PRS-based technique, which provides potentially useful information on changes of molecular alignment in soft tissues due to deformation, aging and disease as well for engineering tissue constructs.

The limitations of this technique arise largely from experimental constraints. The greatest source of error in the experimental setup is the fluorescence interference from tissue, media, and cell culture substrates, though complementary choice of laser, substrate, and spectral range can minimize the background fluorescence [56]. Here, we use a 532nm laser and glass substrate for

tissue samples as glass has a weak background fluorescence at 532nm, despite strong fluorescence at most wavelengths [57]. The contribution of the glass substrate background is strong in the 700-1200 cm^{-1} region (see Figure S2), hence we cut the 600-1300 cm^{-1} region from our analysis to avoid conflation of the signal with the glass background [58]. Though buffer solutions display a strong peak in the 1600-1700 cm^{-1} range, protein peaks are still identifiable after buffer background is subtracted [59]. Hence, spectra in the range we used for post-analysis (1400-1800 cm^{-1}) can be easily subtracted from glass substrates and media (or buffer solutions) without compromising spectral features of cells and proteins. This analytical region contains the CH_2, lipid and phenylalanine bands that are present in many biomacromolecules (e.g., lipids, fatty acid and carbohydrates). More importantly, it contains amide I bands that are present and has been shown sensitive to polarization in many proteins including collagen [16,20], elastin [24], fibroin [60,61] and keratin [62]. Masic et al. [16] found that prominent differences in intensities of Raman bands between 0˚ and 90˚ polarized angles were from the amide I and used the intensity of amide I collagen band for quantifying the anisotropy in tissue. Here, we not only used a single amide I band but the whole amide I region as well as CH_2, lipids and phenylalanine band regions. These regions could vary in different soft tissues of varying protein compositions yet, in our hands, were still able to capture the most significant anisotropy in tissues. Regarding substrate selection, one reason for the strong background signal is that the glass substrate is thick (1000 μm) compared to tissue samples (10 μm). It is acknowledged that thick transparent substrates tend to contribute significant spectral features even when they are out of focus [63]. Another reason for the strong background signal is that the spectra of tissue on glass were acquired with a higher number of accumulations. As a higher number of accumulations will improve the signal to noise ratio for tissue, it also increases the signal of substrate background.

Although we may sacrifice some polarization-sensitive bands (such as Amide III bands) in the 700-1200 cm^{-1} region, we chose to use glass substrates in this study because they are very cheap, versatile and commonly used in cell and tissue work. In future studies, we may consider the usage of more costly substrates (such as CaF_2 and MgF_2) with minimal substrate interference [64]. As to resolution, according to the laws of physics and optics [65], the theoretical diffraction limited spatial resolution was about 1 μm laterally at subcellular scale and the refraction-limited depth resolution [66] was about 6 μm axially in this study. Currently, our probe is integrating over multiple collagen bundles (~300 nm diameter) for a single voxel, which may be contributing to overall PC Score variation. Overall, the sinusoidal variation which we are able to detect is, at best, limited by the true variation that must be encompassed within sample's voxel. Better objectives could increase the spatial and depth resolution up to a wavelength-limited half micron (for a 532nm laser), improve SNR, and potentially decrease variation in analyzed data.

Besides, the effect of fixation and embedding on Raman analysis of soft tissues should be considered. Although the embedded tissue samples may bring the overlap of the embedding medium-related peaks with protein-related peaks [67], the embedding components can be subtracted from spectra of tissues. There are studies working on removing the background of embedding media ((.g., GMA, LR white, and PMMA) as well as paraffin [67,68] from spectra of tissues. Coupled with multivariate analysis methods, Raman spectroscopy has the ability to retain the tissue information from embedded tissue samples. Moreover, our muscle spectra used to derive the master function do not have a peak at 1436 cm^{-1} nor 1441 cm^{-1} (paraffin, CH_2 bending) [69] as shown in Figure 3B. Because the intensity of the residual peak at 1441 cm^{-1} in the loading function is very low, we assume the effect of paraffin residue on the PC1 Score is

negligible. The master loading function ranging from 1400-1800 cm^{-1} should work independent of deparaffinization.

Additional limitations of this method arise from the requirement for measurements at multiple angles, namely inaccurate positioning and long acquisition times. Motorized stages and/or rotation of the polarizer/detector itself could decrease variability associated with the current manual rotation process. Moreover, data acquisition at multiple polarized angles from 0˚-180˚ at sufficient number of regions of interest to overcome natural biological variability requires a long measurement time, especially in cases where there is no prior knowledge of orientation in tissue samples. This makes Raman analysis challenging to implement for living biological samples for future study. In our setup, using the point scan mode where a sample is scanned with a single laser, it took about 4 hours to acquire a complete set of data at all angles for 11 locations in a single ROI. The acquisition time is inflated by the intrinsic fluorescence from tissue that must be overcome for sufficient SNR. To experimentally compensate, the usage of line scan that allows parallel detection of Raman spectra from multiple points simultaneously [70,71] and a higher numerical aperture lens (e.g., N.A.=1) can help decrease the acquisition time for sufficient SNR.

A potential limitation of our method is the relatively large dispersion of PC1 Score per angle. A large dispersion may reduce the anisotropy resolution of this method, which may limit the application of the platform to discern minute differences in sample alignment. Although SNV normalization has been applied to tissue samples to correct for inconsistent thickness, there are other factors that may contribute to dispersion of PC1 Score including spatial distribution and local orientation. For example, the contribution of collagen signal in one location could be slightly different from other locations, which would broaden the dispersion of PC1 Score per

angle. Protein fibers oriented out-of-plane relative to the laser beam axis could also increase the dispersion. The effects of local orientation on PC1 Score can also be seen in the asymmetry of PC1 Scores. The clustering at 0˚ and 30˚ in Fig 4A (and 90˚/120˚/150˚ in Fig 5) are likely due to the existence of a crimp structure at ±30˚ local alignment in highly aligned tissue, e.g., RTT [16]. Since our ultimate goal is to use this method on samples with an unknown alignment magnitude and direction, our current method remains a reasonable way to quantify the overall mesoscale alignment. In future, if we need higher resolution in our amplitude metric to correlate amplitude with intermediate alignment levels, we may consider more sophisticated fitting than the current sine function, e.g., a sigmoid function.

In general, for future application of the Amplitude Alignment Metric to a wide range of tissues and tissue engineered samples, the utility of the master loading function should be verified for more tissue and cell types as well as synthetic biomaterials. The master loading function we have identified could be limited to collagen-rich and muscular samples, though dermal, musculoskeletal and cardiovascular tissues do tend to be of great interest for monitoring macroscale alignment and maturation. In addition, our method has not yet been applied to other scaffolds that are often used in tissue engineering (e.g., polylactic acid and silk). It is likely that a new separate loading function will be required for specific polymers, and a training set of well-aligned polymer would be required. For application to engineered protein-based scaffolds (e.g., cell derived matrices), the utility of master loading to evaluate the alignment level of protein as cells remodel the matrices should also be verified. Although our work here shows a proof of concept to evaluate the capability of the proposed method to quantify anisotropy of processed tissues in a standard histopathology preparation, we also have an interest in applying this method to living tissue and engineered tissue constructs. Development and validation of widely

applicable master loading functions can help researchers to study the impact of processing variables on alignment of tissue-engineered scaffolds and to determine endpoints for harvesting engineered constructs based on their demonstrated level of alignment rather than arbitrary timepoints. To truly monitor the maturation of cell-laden constructs in the future, measurements will have to be conducted at 37℃ in humidity-controlled environments for living samples [72,73]. For such purpose, fresh tissue samples should be characterized. Our current work shows that the statistical significance of PC1 Score between 0˚ and 90˚ was similar for fresh RTT and processed RTT due to similar p-value (see Figure S3), suggesting a minimal effect of chemical processing on the variation of PC1 Score in RTT for amplitude analysis. However, , since are previous studies showing that fixed and deparaffinized tissue samples had reduction in lipid hydrocarbon signals in the spectral region 2800-3000 cm^{-1} [74,75], the effect of fixation and (de)paraffinization protein amide I band of tissues should also be considered in the future. Ultimately, non-destructively monitoring tissue alignment via molecular-level PRS can support tissue engineers in mimicking the physical and mechanical properties of native tissues with organized, hierarchical protein structures.

5. Conclusion

In summary, polarized Raman spectroscopy coupled with PCA analysis offers a non-destructive approach to evaluate anisotropy in soft tissues. Here, we utilized a master loading function from anisotropic tissue that is applied to other tissues with varying concentrations of cells and proteins. We quantified the anisotropy in PRS data by devising an Amplitude Alignment Metric to measure the level of alignment in soft tissues. We showed this PRS-based method had the capability to distinguish anisotropic tissue from isotropic tissue and possessed

similar discriminatory capacity to an FFT-based image processing method. This study extends the utility of PRS to quantify alignment in native tissue and tissue-engineered constructs with varying protein composition, including tissues with complex extracellular matrix proteins.

Declaration of Competing Interest

The authors have no conflicts of interest to declare.

Acknowledgements

The authors acknowledge the support by the National Science Foundation (CMMI 1762791) and the Army Research Office (DURIP Instrumentation Grant ARO-68410-EG-RIP). We also thank Dr. Whitney Stoppel and Dr. Janak Gaire for providing rat tails and mouse skin sections, respectively.

References

[1] R.L. and J.P. Vacanti, Tissue engineering, Science (80-.). 260 (1993) 920–926. https://doi.org/10.1080/00131725009342110.

[2] S.D. Subramony, B.R. Dargis, M. Castillo, E.U. Azeloglu, M.S. Tracey, A. Su, H.H. Lu, The guidance of stem cell differentiation by substrate alignment and mechanical stimulation, Biomaterials. 34 (2013) 1942–1953. https://doi.org/10.1016/j.biomaterials.2012.11.012.

[3] C. Erisken, X. Zhang, K.L. Moffat, W.N. Levine, H.H. Lu, Scaffold fiber diameter regulates human tendon fibroblast growth and differentiation, Tissue Eng. - Part A. 19 (2013) 519–528. https://doi.org/10.1089/ten.tea.2012.0072.

[4] Y. Li, G. Huang, X. Zhang, L. Wang, Y. Du, T.J. Lu, F. Xu, Engineering cell alignment in vitro, Biotechnol. Adv. 32 (2014) 347–365. https://doi.org/10.1016/j.biotechadv.2013.11.007.

[5] Y. Li, Y. Xiao, C. Liu, The Horizon of Materiobiology: A Perspective on Material-Guided Cell Behaviors and Tissue Engineering, Chem. Rev. 117 (2017) 4376–4421. https://doi.org/10.1021/acs.chemrev.6b00654.

[6] L. Van Gulick, C. Saby, H. Morjani, A. Beljebbar, Age-related changes in molecular organization of type I collagen in tendon as probed by polarized SHG and Raman microspectroscopy, Sci. Rep. 9 (2019) 1–12. https://doi.org/10.1038/s41598-019-43636-2.

[7] L. Cao, R. Lafyatis, L.C. Burkly, Increased dermal collagen bundle alignment in systemic sclerosis is associated with a cell migration signature and role of Arhgdib in directed fibroblast migration on aligned ECMs, PLoS One. 12 (2017) 1–15. https://doi.org/10.1371/journal.pone.0180751.

[8] D. Tsiapalis, S. Rana, M. Doulgkeroglou, S. Kearns, J. Kelly, Y. Bayon, D.I. Zeugolis, The effect of aligned electrospun fibers and macromolecular crowding in tenocyte culture, Methods Cell Biol. 157 (2020) 225–247. https://doi.org/10.1016/bs.mcb.2019.11.003.

[9] L.M.S. Loura, Simple estimation of förster resonance energy transfer (FRET) orientation factor distribution in membranes, Int. J. Mol. Sci. 13 (2012) 15252–15270. https://doi.org/10.3390/ijms131115252.

[10] J.D. Rubenstein, P.L. Stanchev, J.K. Kim, R.M. Henkelman, Musculoskeletal Radiology Orientation on MR ofBovine, Radiology. 188 (1993) 219–226.

[11] A.K. Leonard, E.A. Loughran, Y. Klymenko, Y. Liu, O. Kim, M. Asem, K. Mcabee, M.J. Ravosa, M. Sharon, N. Dame, N. Dame, U. States, Methods for the visualization and analysis of extracellular matrix protein structure and degradation, Methods Cell Biol. 143 (2018) 79–95. https://doi.org/10.1016/bs.mcb.2017.08.005.Methods.

[12] B. Yang, N. Jan, B. Brazile, A. Voorhees, K.L. Lathrop, U. States, U. States, Polarized light microscopy for 3D mapping of collagen fiber architecture in ocular tissues, J Biophotonics. 11 (2018) 1–19. https://doi.org/10.1002/jbio.201700356.Polarized.

[13] X. Bi, G. Li, S.B. Doty, N.P. Camacho, A novel method for determination of collagen orientation in cartilage by Fourier transform infrared imaging spectroscopy (FT-IRIS), Osteoarthr. Cartil. 13 (2005) 1050–1058. https://doi.org/10.1016/j.joca.2005.07.008.

[14] G. Bakir, B.E. Girouard, R. Wiens, S. Mastel, E. Dillon, M. Kansiz, K.M. Gough, Orientation Matters: Polarization dependent IR spectroscopy of collagen from intact tendon down to the single fibril level, Molecules. 25 (2020). https://doi.org/10.3390/molecules25184295.

[15] I. Amenabar, S. Poly, W. Nuansing, E.H. Hubrich, A.A. Govyadinov, F. Huth, R. Krutokhvostov, L. Zhang, M. Knez, J. Heberle, A.M. Bittner, R. Hillenbrand, Structural analysis and mapping of individual protein complexes by infrared nanospectroscopy, Nat. Commun. 4 (2013). https://doi.org/10.1038/ncomms3890.

[16] A. Masic, L. Bertinetti, R. Schuetz, L. Galvis, N. Timofeeva, J.W.C. Dunlop, J. Seto, M.A.

Hartmann, P. Fratzl, Observations of multiscale, stress-induced changes of collagen orientation in tendon by polarized Raman spectroscopy, Biomacromolecules. 12 (2011) 3989–3996. https://doi.org/10.1021/bm201008b.

[17] M. Tsuboi, G.J. Thomas, Raman scattering tensors in biological molecules and their assemblies, Appl. Spectrosc. Rev. 32 (1997) 263–299. https://doi.org/10.1080/05704929708003316.

[18] M. Votteler, D.A. Carvajal Berrio, M. Pudlas, H. Walles, K. Schenke-Layland, Non-contact, label-free monitoring of cells and extracellular matrix using Raman spectroscopy, J. Vis. Exp. (2012) 1–7. https://doi.org/10.3791/3977.

[19] G. Falgayrac, S. Facq, G. Leroy, B. Cortet, G. Penel, New method for raman investigation of the orientation of collagen fibrils and crystallites in the haversian system of bone, Appl. Spectrosc. 64 (2010) 775–780. https://doi.org/10.1366/000370210791666255.

[20] M. Janko, P. Davydovskaya, M. Bauer, A. Zink, R.W. Stark, Anisotropic Raman scattering in collagen bundles, Opt. Lett. 35 (2010) 2765. https://doi.org/10.1364/ol.35.002765.

[21] L. Galvis, J.W.C. Dunlop, G. Duda, P. Fratzl, A. Masic, Polarized Raman Anisotropic Response of Collagen in Tendon: Towards 3D Orientation Mapping of Collagen in Tissues, PLoS One. 8 (2013) 1–9. https://doi.org/10.1371/journal.pone.0063518.

[22] M.S. Bergholt, J.P. St-Pierre, G.S. Offeddu, P.A. Parmar, M.B. Albro, J.L. Puetzer, M.L. Oyen, M.M. Stevens, Raman spectroscopy reveals new insights into the zonal organization of native and tissue-engineered articular cartilage, ACS Cent. Sci. 2 (2016) 885–895. https://doi.org/10.1021/acscentsci.6b00222.

[23] M. Jensen, C.C. Horgan, T. Vercauteren, M.B. Albro, M.S. Bergholt, Multiplexed polarized hypodermic Raman needle probe for biostructural analysis of articular cartilage, Opt. Lett. 45 (2020) 2890. https://doi.org/10.1364/ol.390998.

[24] E. Green, R. Ellis, P. Winlove, The molecular structure and physical properties of elastin fibers as revealed by Raman microspectroscopy, Biopolymers. 89 (2008) 931–940. https://doi.org/10.1002/bip.21037.

[25] H. Zhou, C.S. Simmons, M. Sarntinoranont, G. Subhash, Raman Spectroscopy Methods to Characterize the Mechanical Response of Soft Biomaterials, Biomacromolecules. 21 (2020) 3485–3497. https://doi.org/10.1021/acs.biomac.0c00818.

[26] H. Sato, H. Chiba, H. Tashiro, Y. Ozaki, Excitation wavelength-dependent changes in Raman spectra of whole blood and hemoglobin: comparison of the spectra with 514.5-, 720-, and 1064-nm excitation, J. Biomed. Opt. 6 (2001) 366. https://doi.org/10.1117/1.1380668.

[27] A.A. Lykina, D.N. Artemyev, V.I. Kukushkin, I.A. Bratchenko, N.S. Aleksandrov, V.P. Zakharov, Raman spectroscopy for kidney tissue and its neoplasms research, J. Phys. Conf.

Ser. 1096 (2018). https://doi.org/10.1088/1742-6596/1096/1/012116.

[28] M. Haifler, I. Pence, Y. Sun, A. Kutikov, R.G. Uzzo, A. Mahadevan-Jansen, C.A. Patil, Discrimination of malignant and normal kidney tissue with short wave infrared dispersive Raman spectroscopy, J. Biophotonics. 11 (2018) 1–8. https://doi.org/10.1002/jbio.201700188.

[29] R. Gautam, S. Vanga, F. Ariese, S. Umapathy, Review of multidimensional data processing approaches for Raman and infrared spectroscopy, EPJ Tech. Instrum. 2 (2015) 8. https://doi.org/10.1140/epjti/s40485-015-0018-6.

[30] C. Syms, Principal Components Analysis, Encycl. Ecol. Five-Volume Set. (2008) 2940–2949. https://doi.org/10.1016/B978-008045405-4.00538-3.

[31] H. Al Ebrahim, K. Sowoidnich, H. Schmidt, H.-D. Kronfeldt, Polarization Dependence of the Raman Scattering of Oriented Porcine Muscle Fibers Affected by Storage Time and Spoilage, Focus. Mod. Food Ind. 2 (2013) 1–9. www.fmfi-journal.org.

[32] S. Schrof, P. Varga, L. Galvis, K. Raum, A. Masic, 3D Raman mapping of the collagen fibril orientation in human osteonal lamellae, J. Struct. Biol. 187 (2014) 266–275. https://doi.org/10.1016/j.jsb.2014.07.001.

[33] N. Rajan, J. Habermehl, M.F. Coté, C.J. Doillon, D. Mantovani, Preparation of ready-to-use, storable and reconstituted type I collagen from rat tail tendon for tissue engineering applications, Nat. Protoc. 1 (2006) 2753–2758. https://doi.org/10.1038/nprot.2006.430.

[34] B. Burkel, B.A. Morris, S.M. Ponik, K.M. Riching, K.W. Eliceiri, P.J. Keely, Preparation of 3D collagen gels and microchannels for the study of 3D interactions In Vivo, J. Vis. Exp. 2016 (2016) 1–7. https://doi.org/10.3791/53989.

[35] M.P. and R.B.F. Andrew Fitzgibbon, Direct Least Square Fitting of Ellipses, Binggong Xuebao/Acta Armamentarii. 35 (1999) 355–361. https://doi.org/10.3969/j.issn.1000-1093.2014.03.010.

[36] M. Pézolet, M. Pigeon, D. Ménard, J.P. Caillé, Raman spectroscopy of cytoplasmic muscle fiber proteins. Orientational order, Biophys. J. 53 (1988) 319–325. https://doi.org/10.1016/S0006-3495(88)83109-6.

[37] A.S. I Freund, M Deutsch, Connective tissue polarity, Opt. Second. Microsc. Crossed-Beam Summation, Small-Angle Scatt. Rat-Tail Tendon. Biophys. J. 50 (1986) 693–712.

[38] N. Kuhar, S. Sil, T. Verma, S. Umapathy, Challenges in application of Raman spectroscopy to biology and materials, RSC Adv. 8 (2018) 25888–25908. https://doi.org/10.1039/c8ra04491k.

[39] S. Garip, S.H. Bayari, M. Severcan, S. Abbas, I.K. Lednev, F. Severcan, Structural effects of simvastatin on rat liver tissue: Fourier transform infrared and Raman microspectroscopic studies, J. Biomed. Opt. 21 (2016) 025008.

https://doi.org/10.1117/1.jbo.21.2.025008.

[40] T.W. Lin, L. Cardenas, L.J. Soslowsky, Biomechanics of tendon injury and repair, J. Biomech. 37 (2004) 865–877. https://doi.org/10.1016/j.jbiomech.2003.11.005.

[41] J. Uitto, Biochemistry of the elastic fibers in normal connective tissues and its alterations in diseases, J. Invest. Dermatol. 72 (1979) 1–10.

[42] F.E. Uhl, D.E. Wagner, D.J. Weiss, Type I Collagen Purification from Rat Tail Tendons., Methods Mol. Biol. 1627 (2017) 253–283. https://doi.org/10.1007/978-1-4939-7113-8_18.

[43] A. Crovace, L. Lacitignola, G. Rossi, E. Francioso, Histological and immunohistochemical evaluation of autologous cultured bone marrow mesenchymal stem cells and bone marrow mononucleated cells in collagenase-induced tendinitis of equine superficial digital flexor tendon, Vet. Med. Int. 2010 (2010) 1–11. https://doi.org/10.4061/2010/250978.

[44] E. Donnelly, M.G. Ascenzi, C. Farnum, Primary cilia are highly oriented with respect to collagen direction and long axis of extensor tendon, J. Orthop. Res. 28 (2010) 77–82. https://doi.org/10.1002/jor.20946.

[45] A. Jean, G.C. Engelmayr, Anisotropic collagen fibrillogenesis within microfabricated scaffolds: Implications for biomimetic tissue engineering, Adv. Healthc. Mater. 1 (2012) 112–116. https://doi.org/10.1002/adhm.201100017.

[46] T. Novak, S.L. Voytik-Harbin, C.P. Neu, Cell encapsulation in a magnetically aligned collagen-GAG copolymer microenvironment, Acta Biomater. 11 (2015) 274–282. https://doi.org/10.1016/j.actbio.2014.09.031.

[47] C. Ayres, G.L. Bowlin, S.C. Henderson, L. Taylor, J. Shultz, J. Alexander, T.A. Telemeco, D.G. Simpson, Modulation of anisotropy in electrospun tissue-engineering scaffolds: Analysis of fiber alignment by the fast Fourier transform, Biomaterials. 27 (2006) 5524–5534. https://doi.org/10.1016/j.biomaterials.2006.06.014.

[48] S. Polzer, T.C. Gasser, K. Novak, V. Man, M. Tichy, P. Skacel, J. Bursa, Structure-based constitutive model can accurately predict planar biaxial properties of aortic wall tissue, Acta Biomater. 14 (2015) 133–145. https://doi.org/10.1016/j.actbio.2014.11.043.

[49] T. Chen, M.J. Hilton, E.B. Brown, M.J. Zuscik, H.A. Awad, Engineering superficial zone features in tissue engineered cartilage, Biotechnol. Bioeng. 110 (2013) 1476–1486. https://doi.org/10.1002/bit.24799.

[50] K. Yellappa, V. Rakesh, K. Sidu, S. Poddar, A. Kumar, S. Sanjeev, K. Mahto, Combined substrate micropatterning and FFT analysis reveals myotube size control and alignment by contact guidance, (2019) 269–285. https://doi.org/10.1002/cm.21527.

[51] H. Hillman, Limitations of clinical and biological histology, Med. Hypotheses. 54 (2000) 553–564. https://doi.org/10.1054/mehy.1999.0894.

[52] K.L. Camplejohn, S.A. Allard, Limitations of safranin “O” staining in proteoglycan-depleted cartilage demonstrated with monoclonal antibodies, Histochemistry. 89 (1988) 185–188. https://doi.org/10.1007/BF00489922.

[53] A. Zoladek, F. Pascut, P. Patel, I. Notingher, Development of Raman Imaging System for time-course imaging of single living cells, Spectroscopy. 24 (2010) 131–136. https://doi.org/10.3233/SPE-2010-0410.

[54] J.M. Surmacki, B.J. Woodhams, A. Haslehurst, B.A.J. Ponder, S.E. Bohndiek, Raman micro-spectroscopy for accurate identification of primary human bronchial epithelial cells, Sci. Rep. 8 (2018) 1–11. https://doi.org/10.1038/s41598-018-30407-8.

[55] M.J. Mondrinos, F. Alisafaei, A.Y. Yi, H. Ahmadzadeh, I. Lee, C. Blundell, J. Seo, M. Osborn, T.J. Jeon, S.M. Kim, V.B. Shenoy, D. Huh, Surface-directed engineering of tissue anisotropy in microphysiological models of musculoskeletal tissue, Sci. Adv. 7 (2021). https://doi.org/10.1126/SCIADV.ABE9446.

[56] H.J. Butler, L. Ashton, B. Bird, G. Cinque, K. Curtis, J. Dorney, K. Esmonde-White, N.J. Fullwood, B. Gardner, P.L. Martin-Hirsch, M.J. Walsh, M.R. McAinsh, N. Stone, F.L. Martin, Using Raman spectroscopy to characterize biological materials, Nat. Protoc. 11 (2016) 664–687. https://doi.org/10.1038/nprot.2016.036.

[57] N. Byrne, H.J., Sockalingum, G. & Stone, Biomedical applications of synochroton infrared microspectroscopy: A practical approach, Royal Society of Chemistry, 2011.

[58] S. Wang, J. Zhao, H. Lui, Q. He, H. Zeng, A modular Raman microspectroscopy system for biological tissue analysis, Spectroscopy. 24 (2010) 577–583. https://doi.org/10.3233/SPE-2010-0487.

[59] A.E. Baker, A.R. Mantz, M.L. Chiu, Raman spectroscopy characterization of antibody phases in serum, MAbs. 6 (2014) 1509–1517. https://doi.org/10.4161/19420862.2014.975100.

[60] T. Lefèvre, M.E. Rousseau, M. Pézolet, Orientation-insensitive spectra for raman microspectroscopy, Appl. Spectrosc. 60 (2006) 841–846. https://doi.org/10.1366/000370206778062039.

[61] T. Lefèvre, M.E. Rousseau, M. Pézolet, Protein secondary structure and orientation in silk as revealed by Raman spectromicroscopy, Biophys. J. 92 (2007) 2885–2895. https://doi.org/10.1529/biophysj.106.100339.

[62] R. ¨el P. and P. Colomban, Nanomechanics of single keratin fibres: A Raman study of the a-helix → b-sheet transition and the effect of water, J. Raman Spectrosc. 38 (2007) 1538–1553. https://doi.org/10.1002/jrs.

[63] N.J. Everall, Confocal Raman microscopy: Performance, pitfalls, and best practice, Appl. Spectrosc. 63 (2009). https://doi.org/10.1366/000370209789379196.

[64] L.T. Kerr, H.J. Byrne, B.M. Hennelly, Optimal choice of sample substrate and laser wavelength for Raman spectroscopic analysis of biological specimen, Anal. Methods. 7 (2015) 5041–5052. https://doi.org/10.1039/c5ay00327j.

[65] C.B. Juang, L. Finzi, C.J. Bustamante, Design and application of a computer-controlled confocal scanning differential polarization microscope, Rev. Sci. Instrum. 59 (1988) 2399–2408. https://doi.org/10.1063/1.1139918.

[66] N.J. Everall, Confocal Raman microscopy: Why the depth resolution and spatial accuracy can be much worse than you think, Appl. Spectrosc. 54 (2000) 1515–1520. https://doi.org/10.1366/0003702001948439.

[67] Y.N. Yeni, J. Yerramshetty, O. Akkus, C. Pechey, C.M. Les, Effect of fixation and embedding on Raman spectroscopic analysis of bone tissue, Calcif. Tissue Int. 78 (2006) 363–371. https://doi.org/10.1007/s00223-005-0301-7.

[68] P. Meksiarun, M. Ishigaki, V.A.C. Huck-Pezzei, C.W. Huck, K. Wongravee, H. Sato, Y. Ozaki, Comparison of multivariate analysis methods for extracting the paraffin component from the paraffin-embedded cancer tissue spectra for Raman imaging, Sci. Rep. 7 (2017) 1–10. https://doi.org/10.1038/srep44890.

[69] R. Gaifulina, A.T. Maher, C. Kendall, J. Nelson, M. Rodriguez-Justo, K. Lau, G.M. Thomas, Label-free Raman spectroscopic imaging to extract morphological and chemical information from a formalin-fixed, paraffin-embedded rat colon tissue section, Int. J. Exp. Pathol. 97 (2016) 337–350. https://doi.org/10.1111/iep.12194.

[70] M. Okuno, H. Hamaguchi, Multifocus confocal Raman microspectroscopy for fast multimode vibrational imaging of living cells, Opt. Lett. 35 (2010) 4096. https://doi.org/10.1364/ol.35.004096.

[71] K. Hamada, K. Fujita, M. Kobayashi, S. Kawata, Observation of cell dynamics by laser scanning Raman microscope, Three-Dimensional Multidimens. Microsc. Image Acquis. Process. XIV. 6443 (2007) 64430Z. https://doi.org/10.1117/12.700729.

[72] I. Notingher, L.L. Hench, Raman microspectroscopy: A noninvasive tool for studies of individual living cells in vitro, Expert Rev. Med. Devices. 3 (2006) 215–234. https://doi.org/10.1586/17434440.3.2.215.

[73] R. Smith, K.L. Wright, L. Ashton, Raman spectroscopy: An evolving technique for live cell studies, Analyst. 141 (2016) 3590–3600. https://doi.org/10.1039/c6an00152a.

[74] B. Brozek-Pluska, M. Kopec, J. Surmacki, H. Abramczyk, Histochemical analysis of human breast tissue samples by IR and Raman spectroscopies. Protocols discussion, Infrared Phys. Technol. 93 (2018) 247–254. https://doi.org/10.1016/j.infrared.2018.08.005.

[75] J. Depciuch, E. Kaznowska, K. Szmuc, I. Zawlik, M. Cholewa, P. Heraud, J. Cebulski, Comparing paraffined and deparaffinized breast cancer tissue samples and an analysis of Raman spectroscopy and infrared methods, Infrared Phys. Technol. 76 (2016) 217–226.

https://doi.org/10.1016/j.infrared.2016.02.006.